American Mineralogist, Volume 89, pages 601–609, 2004

Structure and crystallization behavior of the (Ba,Sr)$HAsO_4 \cdot H_2O$ solid-solution in aqueous environments

AMALIA JIMÉNEZ,[1,*] MANUEL PRIETO,[1] MIGUEL ÁNGEL SALVADÓ,[2] AND SANTIAGO GARCÍA-GRANDA[2]

[1]Departamento de Geología, c/ Jesús Arias de Velasco, s/n, 33005 Oviedo, Spain
[2]Departamento de Química Física y Analítica, c/ Julián Clavería 8, 33006 Oviedo, Spain

ABSTRACT

Crystals of different members of the (Ba,Sr)$HAsO_4 \cdot H_2O$ solid solution have been synthesized, and the first structural studies indicate that they crystallize in the same space group, *Pbca*, with $Z = 8$. The unit-cell parameters are $a = 7.436(2)$, $b = 8.481(1)$, $c = 14.348(6)$ Å, and $a = 7.752(1)$, $b = 8.759(1)$, $c = 14.668(3)$ Å for the strontium and barium end-members, respectively. Both end-members have a layered structure with slices parallel to (001) linked by hydrogen bonds from the water molecules. These features are consistent with both the perfect cleavage on {001} and the morphological importance of this form in the crystals obtained. However, the two end-members are not isostructural and show differences in both the anionic hydrogen positions and number of hydrogen bonds. Complementary powder-diffraction measurements indicate that the cell parameters increase in a non-linear way with the barium content indicating that the solid solution is complete but could be non-ideal. Preliminary data suggest that barium partitions preferentially into the solid phase when crystallizing this solid solution from aqueous solutions.

INTRODUCTION

Although arsenic has been classified at the top of the priority list of the most hazardous substances (Nriagu 1994; Smedley and Kinniburgh 2002), the crystal structures of numerous arsenates remain poorly determined. This is an important handicap because an in-depth study of the arsenate behavior in soils, sediments, and natural waters that have been subjected to pollution requires a precise knowledge of the possible precipitating phases, their crystal chemistry, and their thermodynamic properties. Furthermore, in multi-component aqueous systems, the precipitation of solid solutions is always a possibility (Glynn and Reardon 1990; Prieto et al. 1997) such that the study of arsenate solid solutions involving substitution between atoms of similar size and character is worthwhile. With this focus we have studied the crystal chemistry and crystallization behavior of the (Ba,Sr)$HAsO_4 \cdot H_2O$ solid-solution. Previous studies (Planer-Friedrich et al. 2001) indicate that, at high concentrations, compounds in this series could be a limiting phase for arsenic in natural aqueous environments. The only available data on this series correspond to the strontium end-member, whose space group (*Pbca*), cell parameters, and atomic positions of Sr and As were determined by Binas and Boll-Dornberger (1962). From powder diffraction data, Martin et al. (1970) determine the same space group for the barium end-member and suggest that $SrHAsO_4 \cdot H_2O$ and $BaHAsO_4 \cdot H_2O$ are isomorphous and therefore good candidates to form solid solutions. However, given that the location of hydrogen and O atoms and water molecules in these structures is unresolved, the isostructural character of these compounds needs to be confirmed.

At present, the most complete study on the crystal chemistry of hydrated acidic arsenates has been carried out by Ferraris and co-workers, who survey the stereochemistry of the $[HAsO_4]^{2-}$ group and the structural role of the water molecules in $Na_2HAsO_4 \cdot 7H_2O$ (Ferraris and Chiari 1970; Ferraris et al. 1971a), haidingerite ($CaHAsO_4 \cdot H_2O$; Ferraris et al. 1972), and pharmacolite ($CaHAsO_4 \cdot 2H_2O$; Ferraris et al. 1971b). According to these authors, some structural features seem to be common in these hydrated acidic arsenates. This is particularly evident for the $(HAsO_4)^{2-}$ group, in which the acidic hydrogen atom is invariably bonded to the O atom with an As-O distance clearly longer than the other three in the AsO_4 tetrahedra. The H-O distance in this bond is slightly longer than the H-Ow distances, where Ow represents the O atom in a water molecule. Moreover, each anionic hydrogen atom forms a non-linear hydrogen bond to an O atom of the nearest $HAsO_4^{2-}$ group in the structure, with dimensions (distances and angles) that are fairly similar in these three compounds. However, other important features vary significantly from one compound to the other. In general terms, the previous studies on acidic arsenate hydrates demonstrate the adaptability of both the water molecules and hydrogen bridges to facilitate packing in a particular structural environment. In the present context, these features suggest that small differences in atomic sites and hydrogen bonding could produce deviations from perfect isomorphism between $SrHAsO_4 \cdot H_2O$ and $BaHAsO_4 \cdot H_2O$, which in turn could affect the nature of the miscibility between both end-members. In view of these observations, a single-crystal X-ray diffraction study of $SrHAsO_4 \cdot H_2O$, $BaHAsO_4 \cdot H_2O$, and one intermediate composition has been undertaken such that the position of water molecules and anionic hydrogen atoms could be determined and the stereochemistry of the $(HAsO_4)^{2-}$ groups established. In addition to the structural resolution, a study of the crystallization behavior of (Ba,Sr)$HAsO_4 \cdot H_2O$ solid solutions from aqueous solutions, including determination of distribution coefficients and morphological features, has been performed.

* E-mail: amalia.jimenez@geol.uniovi.es

EXPERIMENTAL METHODS

Single crystals of different compositions within the (Sr,Ba)$HAsO_4{\cdot}H_2O$ solid-solution were synthesized at 25 ± 0.1 °C in a counter-diffusion-reaction system. The experimental device consists of a U-shaped tube where two source reservoirs (8 cm^3) are separated by a diffusion column (9 mm diameter and 280 mm long) of silica hydrogel. This method has been extensively used as a way of growing crystals of sparingly soluble salts (Henisch 1988; Lefaucheux and Robert 1994; Prieto et al. 1994) and has also been applied to study crystallization of solid solutions from aqueous solutions (Prieto et al. 1997). In this particular case, one of the source reservoirs was filled with a $Na_2HAsO_4{\cdot}7H_2O$ (0.1 *M*) parent solution and the other with an aqueous solution of $BaCl_2$ and $SrCl_2$. To obtain different compositional terms in this series, a set of experiments with different concentrations of barium and strontium was carried out. Reagent grade chemicals (Merk) were used in all the experiments. The silica hydrogel was prepared by acidification of a sodium silicate (Na_2SiO_3) aqueous solution (Merck, sp. gr.: 1.059 g/cm^3; pH 11.2) with HCl (1 *N*) until pH = 5.5 was attained. The gel obtained is a porous medium that contains 95.6% water within interconnecting pores. Before the experiment starts, the gel column is a homogeneous medium with zero reagent concentration. However, as a result of diffusion of the reagents, the column becomes heterogeneous and develops concentration gradients. Finally, the counter-diffusing reacting ions meet and precipitate in a narrow region of the diffusion column. The precipitating crystals, with sizes ranging from 0.1 to 1.5 mm, were extracted from the column and studied with a scanning electron microscope (SEM, JEOL-6100) equipped with an energy-dispersive X-ray (EDX) spectrometer (Oxford Instruments). Finally, representative individuals were selected for the X-ray diffraction study.

The crystal structure of the strontium end-member ($SrHAsO_4{\cdot}H_2O$) was solved using Patterson and Fourier techniques. Throughout the experiment, Mo$K\alpha$ radiation was used with a graphite crystal monochromator on a Nonius CAD-4 single crystal diffractometer (λ = 0.71073 Å). The unit-cell dimensions were determined from the angular settings of 25 reflections with θ between 15 and 20°. The space group was determined to be *Pbca* from the systematic absences. The intensity data of 1567 "unique" reflections ($0° < \theta < 32°$) were measured using the ω-2θ scan technique with a maximum scan time of 60 s per reflection. The intensity of the primary beam was checked throughout the data collection by monitoring three standard reflections every 60 min from which final drift correction factors were obtained. Profile analysis was performed (Lehman and Larsen 1974; Grant and Gabe 1978) on all of the reflections. Lorentz and polarization corrections were applied and the data were reduced to F^2 values. The structure was solved with Patterson methods using the DIRDIF program (Beurskens et al. 1992). Isotropic least-squares refinement was carried out using the SHELXL97 program (Sheldrick 1997) and an empirical absorption correction was applied using XABS2 (Parkin et al. 1995). During the final stages of the refinement, the positional parameters and the anisotropic thermal parameters of non-H atoms were refined. The positions of hydrogen atoms were determined using difference Fourier synthesis and refined isotropically using distance restraints. Pertinent data collection and refinement parameters are given in Table 1. Geometrical calculations were made with PARST (Nardelli 1983).

The crystal structure of the barium end-member ($BaHAsO_4{\cdot}H_2O$) was solved and refined using a similar procedure (see Table 1). In this case, however, hydrogen atoms were determined using difference Fourier synthesis and isotropically refined by allowing the anionic H1 atom to ride on O1 and freely rotate around the As-O1 bond. The water molecule was refined as a rigid group. Finally, the crystal structure of one intermediate member was refined starting from the structural model of the nearest end-member and introducing an occupancy factor for the Ba/Sr site. Experimental details and parameters for this intermediate composition are also summarized in Table 1.

The single-crystal study of these three members was complemented with an X-ray powder-diffraction study of several intermediate compositions. Diffraction data were collected at room temperature with a Philips X'Pert PRO powder diffractometer, using monochromatic Cu$K\alpha_1$ radiation (λ = 1.5405 Å) and covering a range of $10° \geq 2\theta \geq 40°$ with a step size of 2θ = 0.02° and a time per step of 5 s. For each spectrum, several peaks were indexed by comparison with the diffraction pattern of the closest end-member (computed from the structural data). The refinement of the unit cell parameters was done with a least-squares fit through the angular differences between measured peaks and indexed reflections, using the X'Pert Plus v.1.0 program (Philips Electronics).

RESULTS

Crystal structures

Details of data collection, refinement parameters, and lattice parameters are given in Table 1. Fractional atomic coordinates and equivalent isotropic displacement parameters are given in Table 2. Anisotropic atomic displacement parameters for all non-H atoms are given in Table 3. Finally, Tables 4, 5, and 6 contain selected interatomic distances and bond angles for $SrHAsO_4{\cdot}H_2O$, $Sr_{0.89}Ba_{0.11}HAsO_4{\cdot}H_2O$, and $BaHAsO_4{\cdot}H_2O$, respectively. All three solids crystallize in the orthorhombic space group *Pbca* with cell parameters increasing with the barium concentration in the solid phase. The number of formula units per unit cell is the same (eight) for all three samples and the heavy atoms are arranged in comparable general positions. However, the results reveal significant differences in the position of the acidic hydrogen atoms and consequently in the distribution of hydrogen bonds.

Figure 1 shows the projection, onto (100), of a region of the $SrHAsO_4{\cdot}H_2O$ structure in which both the configuration of the $[HAsO_4]^{2-}$ group and the coordination around a strontium atom can be observed. Arsenic is coordinated with four O atoms to form an irregular tetrahedron where the O-As-O angles vary between 102.02 and 115.17° (Table 4). One of these O atoms is attached to a hydrogen atom at a distance O1-H1 = 0.73 (6) Å, thereby forming the acid-arsenate $[HAsO_4]^{2-}$ group. The distance from this O atom to the central arsenic atom, As-O1 = 1.744 (3) Å, is clearly longer than the other three As-O distances, i.e., the anionic hydrogen H1 is attached to the O atom farthest from arsenic in the tetrahedron. The O atoms O2 and O4 are at similar distances (≈ 1.675 Å) from the central arsenic atom, being ac-

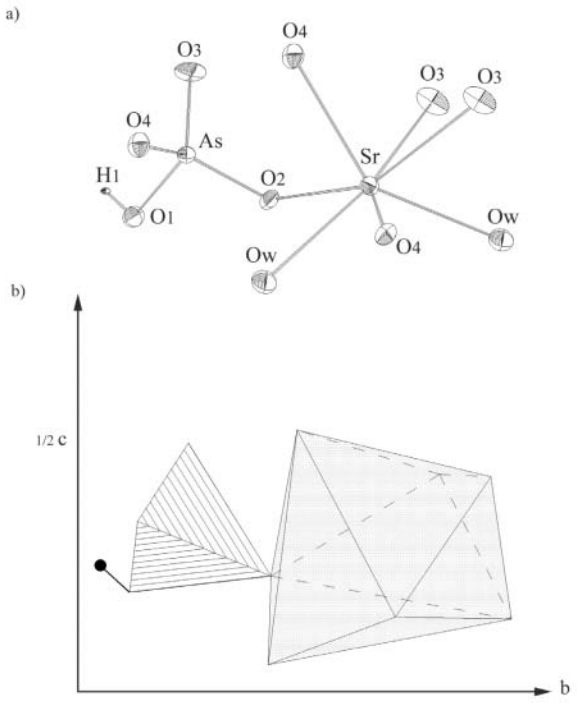

FIGURE 1. Projection of a region of the $SrHAsO_4{\cdot}H_2O$ structure onto (100). The O1 atom of the arsenate group is attached to H1, thereby forming the acidic arsenate $[HAsO_4]^{2-}$ group. The strontium atom is surrounded by five arsenate O atoms and by two Ow atoms from water molecules. (**a**) ORTEP-style plot. (**b**) Arsenate tetrahedron and seven-apex polyhedron around the strontium atom. The anionic hydrogen atom (small black circle) is also shown.

TABLE 1. Experimental details

	$SrHAsO_4·H_2O$	$(Sr_{0.89}Ba_{0.11})HAsO_4·H_2O$	$BaHAsO_4·H_2O$
Chemical formula	$SrHAsO_4·H_2O$	$Sr_{0.89}Ba_{0.11}HAsO_4·H_2O$	$BaHAsO_4·H_2O$
Formula weight	245.56	250.97	295.28
System, Space Group	Orthorhombic, *Pbca*	Orthorhombic, *Pbca*	Orthorhombic, *Pbca*
a, *b*, *c* (Å)	7.4361(17), 8.4808(15), 14.348(6)	7.443(3), 8.477(8), 14.38(5)	7.7519(11), 8.759(14), 14.668(3)
V (Å)^3	904.8(5)	908(3)	996(2)
Z	8	8	8
D (mg·m^{-3})	3.61	3.67	3.94
Radiation type, λ (Å)	Mo*K*α, 0.71073	Mo*K*α, 0.71073	Mo*K*α, 0.71073
No. reflections for cell parameters	25	25	25
μ (mm^{-1})	19.084	18.687	14.487
F (000)	912	928	1056
Temperature (K)	293(2)	293(2)	293(2)
Crystal color	colorless	colorless	colorless
Crystal size	0.46 × 0.10 × 0.10	0.26 × 0.13 × 0.10	0.36 × 0.23 × 0.17
Diffractometer	Nonius CAD-4	Nonius CAD-4	Nonius CAD-4
Data collection method	ω-2θ	ω-2θ	ω-2θ
No. collected reflections	1566	1567	1719
θ range (°) max	31.97	31.95	31.95
Range of *h*, *k*, *l*	$0 \le h \le 11$ $0 \le k \le 12$ $0 \le l \le 21$	$0 \le h \le 11$ $0 \le k \le 12$ $0 \le l \le 21$	$0 \le h \le 11$ $0 \le k \le 13$ $0 \le l \le 21$
Refinement method	Full-matrix least-squares on F^2	Full-matrix least-squares on F^2	Full-matrix least-squares on F^2
Goodness of fit on F^2	1.070	1.026	1.151
No. of reflections, restraints, and parameters used in the refinement	1566/3/76	1567/4/77	1719/0/69
R indices, *wR*2,	0.029 [for 1065 × *I* > 2σ(*I*)], 0.0705	0.033[for 1039 × *I* > 2σ(*I*)], 0.0805	0.046[for 1474 × *I* > 2σ(*I*)], 0.1236
R indices (all data), *wR*2	0.0623, 0.0791	0.0783, 0.0924	0.0539, 0.1277
Weighting scheme*:	*w*1 = 0.033 *w*2 = 3.9	*w*1 = 0.051 w2 = 0.6	w1 = 0.075 w2 = 11.2
$\Delta\rho_{max}$, $\Delta\rho_{min}$ (e Å^{-3})	0.937, −1.389	1.393, −1.04	1.755, −3.925

* $w = 1 / [\sigma^2(F_o^2) + (w1 \times P)^2 + (w2 \times P)]$, where $P = [\mathrm{Max}(F_o^2, 0) + 2 \times F_c^2) / 3$.

ceptors of a hydrogen bond from a water molecule. The O3 atom is the closest to the arsenic atom with As-O3 = 1.665 (3) Å, and is not involved in any hydrogen bonding. All of these features illustrate the distortion of the tetrahedron in the $[HAsO_4]^{2-}$ group, in which only the angle O3-As-O4 = 109.7(2)° is close to the O-T-O angles of a regular tetrahedron. Finally, considering the nearest neighbors, the strontium atoms are surrounded by five O atoms of adjacent acid-arsenate groups and by two Ow atoms of water molecules (Fig. 1a), with distances ranging from 2.563(3) to 2.744(4) Å. An irregular seven-apex (SrO_7) polyhedron can be used to describe the coordination (Fig. 1b). The hydroxyl O1-H1 apices are the only ones in the acid-arsenate tetrahedra that are not shared with these (SrO_7) polyhedra. The O2 atoms connect each tetrahedron with one seven-apex (SrO_7) polyhedron. Finally, each one of the other two O atoms of the tetrahedra, O3 and O4, are shared simultaneously with two [SrO_7] polyhedra.

The hydrogen-bonding network is shown in Figure 2. Both the water hydrogen atoms and the anionic hydrogen atoms are involved in hydrogen bridges, which gives three hydrogen bonds per unit formula in the $SrHAsO_4·H_2O$ structure. Each anionic H1 atom forms a non-linear hydrogen bond to an O2 atom of the nearest arsenate group in the structure, with an O1-H1···O2 angle of 173 (7)° and an H1···O2 distance of 1.92 (6) Å (Table 4). Moreover, the hydrogen atoms of each water molecule form two hydrogen bridges in which the acceptors are O atoms of two arsenate groups, with distances H2···O4 = 1.98(7) Å and H3···O2 = 1.89(3) Å. Thus, water molecules alternate with arsenate groups to form zigzag chains in the [010] direction (Fig. 2a). In these chains, the group consisting of one water molecule and the corresponding acceptor O atoms is not planar. These

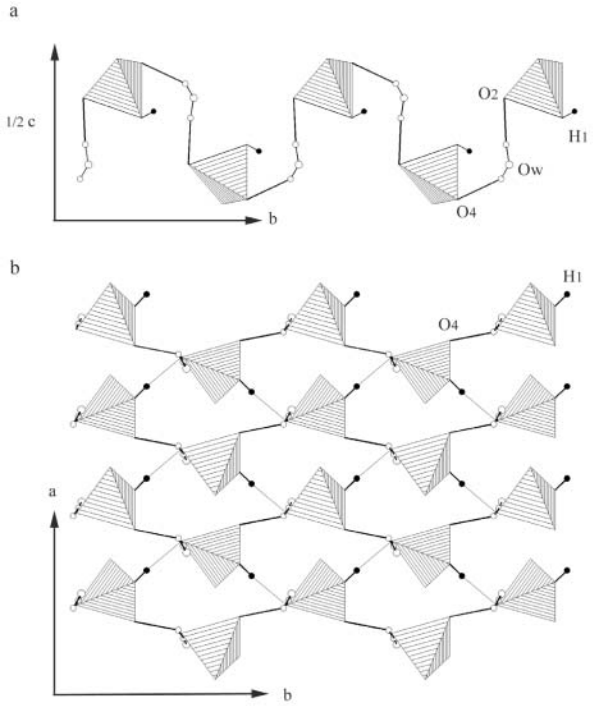

FIGURE 2. Hydrogen bonds in the $SrHAsO_2·H_2O$ structure. (**a**) Arsenate groups and water molecules link to form zigzag chains along [010]. (**b**) Hydrogen atoms link zigzag chains to form slices parallel to (001). Hydrogen bonds involving water hydrogen atoms (small open circles) are represented by thick solid lines. Hydrogen bonds involving anionic hydrogen atoms (black circles) are represented by thin lines.

TABLE 2. Fractional atomic coordinates and equivalent isotropic displacement parameters ($Å^2 \times 10^3$) for three members of the (Sr,Ba)$HAsO_4 \cdot H_2O$ solid solution

	x	*y*	*z*	U_{eq}
$SrHAsO_4 \cdot H_2O$				
Sr	–0.3618 (1)	0.1819 (1)	0.0814 (1)	12 (1)
As	0.1450 (1)	0.0540 (1)	0.1125 (1)	10 (1)
O1	0.2011 (6)	0.1591 (4)	0.2128 (2)	19 (1)
O2	0.0758 (5)	–0.1181 (4)	0.1564 (2)	15 (1)
O3	0.3277 (4)	0.0424 (4)	0.0457 (3)	21 (1)
O4	–0.0136 (5)	0.1592 (4)	0.0578 (2)	17 (1)
Ow	0.8618 (5)	0.0940 (4)	0.6561 (2)	22 (1)
H1	0.265 (9)	0.216 (7)	0.194 (4)	20 (2)
H2	0.940 (8)	0.133 (9)	0.616 (4)	6 (3)
H3	0.897 (9)	0.109 (8)	0.713 (2)	5 (2)
$(Sr_{0.89}Ba_{0.11})HAsO_4 \cdot H_2O$				
Sr	-0.3616 (1)	0.1820 (1)	0.0813 (1)	14 (1)
Ba	-0.3616 (1)	0.1820 (1)	0.0813 (1)	14 (1)
As	0.1451 (1)	0.0539 (1)	0.1125 (1)	10 (1)
O1	0.2019 (6)	0.1587 (4)	0.2133 (2)	18 (1)
O2	0.0760 (5)	-0.1172 (4)	0.1559 (2)	16 (1)
O3	0.3270 (5)	0.0418 (5)	0.0463 (3)	23 (1)
O4	-0.0124 (5)	0.1596 (4)	0.0578 (3)	17 (1)
Ow	0.8616 (6)	0.0939 (4)	0.6560 (3)	22 (1)
H1	0.2720 (6)	0.2410 (4)	0.2070 (4)	13 (13)
H2	0.9630 (7)	0.1300 (11)	0.6320 (4)	110 (4)
H3	0.8710 (8)	0.0920 (8)	0.717 (1)	40 (2)
$BaHAsO_4 \cdot H_2O$				
Ba	–0.3609 (1)	0.1854 (1)	0.0822 (1)	10 (1)
As	0.1513 (1)	0.0594 (1)	0.1128 (1)	7 (1)
O1	0.2140 (8)	0.1582 (1)	0.2112 (3)	18 (1)
O2	0.0906 (6)	–0.1104 (5)	0.1539 (3)	13 (1)
O3	0.3166 (6)	0.0544 (6)	0.0413 (3)	17 (1)
O4	–0.0094 (6)	0.1609 (6)	0.0660 (3)	14 (1)
Ow	0.8798 (7)	0.0951 (5)	0.6626 (3)	16 (1)
H1	0.1687	0.2429	0.2116	90 (3)
H2	–0.5369	0.3492	0.3728	90 (3)
H3	–0.5413	0.4220	0.2824	90 (3)

Note: U_{eq} is defined as one-third of the trace of the orthogonalized U_{ij} tensor.

TABLE 3. Anisotropic displacement parameters ($Å^2 \times 10^3$) for three members of the (Sr,Ba)$HAsO_4 \cdot H_2O$ solid solution

	U_{11}	U_{22}	U_{33}	U_{23}	U_{13}	U_{12}
$SrHAsO_4 \cdot H_2O$						
Sr	11 (1)	12 (1)	13 (1)	–2 (1)	–1 (1)	2 (1)
As	11 (1)	11(1)	9 (1)	0 (1)	0 (1)	0 (1)
O1	27 (2)	16 (2)	12 (2)	–3 (1)	1 (1)	–9 (1)
O2	22 (2)	12 (1)	11 (1)	3 (1)	1 (1)	–3 (1)
O3	10 (2)	34 (2)	20 (2)	–10 (2)	8 (1)	–7 (1)
O4	18 (2)	15 (2)	18 (2)	3 (1)	–3 (1)	3 (1)
O5	33 (2)	20 (2)	13 (2)	2 (1)	1 (2)	0 (2)
$(Sr_{0.89}Ba_{0.11})HAsO_4 \cdot H_2O$						
Sr	15 (1)	15 (1)	13 (1)	–2 (1)	–1 (1)	2 (1)
Ba	15 (1)	15 (1)	13 (1)	–2 (1)	–1 (1)	2 (1)
As	13 (1)	12 (1)	7 (1)	0 (1)	1 (1)	0 (1)
O1	28 (2)	19 (2)	7 (2)	–4 (1)	1 (2)	–8 (2)
O2	22 (2)	11 (1)	14 (2)	3 (1)	1 (2)	–1 (1)
O3	16 (2)	32 (2)	20 (2)	-8 (2)	7 (2)	–9 (2)
O4	19 (2)	17 (2)	14 (2)	1 (1)	–4 (1)	6 (1)
O5	32 (2)	21 (2)	12 (2)	1 (2)	4 (2)	2 (2)
$BaHAsO_4 \cdot H_2O$						
Ba	10 (1)	11 (1)	8 (1)	–1 (1)	0 (1)	1 (1)
As	9 (1)	8 (1)	5 (1)	0 (1)	0(1)	0 (1)
O1	33 (3)	16 (2)	7 (2)	–2 (2)	-1 (2)	–6 (2)
O2	18 (2)	9 (2)	12 (2)	2 (2)	-3 (2)	–6 (2)
O3	10 (2)	27 (2)	15 (2)	–8 (2)	7 (2)	–4 (2)
O4	13 (2)	13 (2)	16 (2)	6 (2)	0 (2)	4 (2)
O5	26 (2)	14 (2)	7 (2)	2 (2)	0 (2)	–1 (2)

Note: The anisotropic displacement factor exponent takes the form: $-2\pi^2 (h^2 a^{*2} U_{11} + \ldots + 2 h k a^* b^* U_{12})$.

TABLE 4. Atomic distances (Å) and angles (°) for $SrHAsO_4 \cdot H_2O$

HAsO4 group	Hydrogen bonds	Strontium coordination
As–O1 = 1.744(3)	Ow–H2 = 0.88(2)	Sr–O2 no. 1 = 2.563(3)
As–O2 = 1.671(3)	Ow–H3 = 0.87(2)	Sr–Ow no. 2 = 2.573(4)
As–O3 = 1.665(3)	H1····O2 = 1.92(6)	Sr–O4 = 2.618(4)
As–O4 = 1.674(3)	H2····O4 = 1.98(7)	Sr–O3 no. 3 = 2.644(3)
O1–H1 = 0.73(6)	H3····O2 = 1.89(3)	Sr–O3 no. 4 = 2.647(4)
O2–As–O1 = 102.0(2)	O1····O2 = 2.642(5)	Sr–O4 no. 5 = 2.661(4)
O4–As–O1 = 106.4(2)	Ow····O4 = 2.688(5)	Sr–Ow no. 6 = 2.744(4)
O3–As–O1 = 108.0(2)	Ow····O2 = 2.737(5)	
O3–As–O4 = 109.7(2)	O4····Ow····O2 = 113.51	
O3–As–O2 = 114.7(2)	O1–H1····O2 = 173(7)	
O2–As–O4 = 115.2(2)	Ow–H2····O4 = 137(5)	
	Ow–H3····O2 = 167(3)	

Notes: No. 1 = $-x - 1/2, y + 1/2, z$; no. 2 = $-x + 1/2, -y, z - 1/2$; no. 3 = $x - 1, y, z$; no. 4 = $-x, -y, -z$; no. 5 = $x - 1/2, -y + 1/2, -z$; no. 6 = $x - 1, -y + 1/2, z - 1/2$. Hydrogen bridges are denoted by points (····).

TABLE 5. Atomic distances (Å) and angles (°) for $Sr_{0.89}Ba_{0.11}HAsO_4 \cdot H_2O$

HAsO4 group	Hydrogen bonds	Strontium coordination
As–O1 = 1.752(5)	Ow–H2 = 0.88(6)	Sr–O2 no. 1 = 2.569(4)
As–O2 = 1.661(4)	Ow–H3 = 0.88(2)	Sr–Ow no. 2 = 2.573(5)
As–O3 = 1.658(4)	H1····O2 = 1.81(5)	Sr–O4 = 2.628(4)
As–O4 = 1.672(4)	H2····O4 = 2.09(9)	Sr–O3 no. 3 = 2.651(6)
O1–H1 = 0.88(2)	H3····O2 = 1.88(3)	Sr–O3 no. 4 = 2.653(4)
O2–As–O1 = 101.9(2)	O1····O2 = 2.65(5)	Sr–O4 no. 5 = 2.658(6)
O4–As–O1 = 106.6(2)	Ow····O4 = 2.69(6)	Sr–Ow no. 6 = 2.744(4)
O3–As–O1 = 108.0(2)	Ow····O2 = 2.75(1)	
O3–As–O4 = 109.6(3)	O4····Ow····O2 = 113.66	
O3–As–O2 = 114.5(2)	O1–H1····O2 = 162(4)	
O2–As–O4 = 115.3(2)	Ow–H2····O4 = 125(6)	
	Ow–H3····O2 = 170(2)	

Notes: No. 1 = $-x - 1/2, y + 1/2, z$; no. 2 = $-x + 1/2, -y, z - 1/2$; no. 3 = $-x, -y, -z$; no. 4 = $x - 1, y, z$; no. 5 = $x - 1/2, -y + 1/2, -z$; no. 6 = $x - 1, -y + 1/2, z - 1/2$. Hydrogen bridges are denoted by points (····).

TABLE 6. Atomic distances (Å) and angles (°) for $BaHAsO_4 \cdot H_2O$

HAsO4 group	Hydrogen bonds	Strontium coordination
As–O1 = 1.753(5)	Ow–H2 = 1.0236	Ba–Ow no. 1 = 2.729(6)
As–O2 = 1.673(5)	Ow–H3 = 0.9616	Ba–O2 no. 2 = 2.734(5)
As–O3 = 1.656(5)	H2····O4 = 1.891(5)	Ba–O4 = 2.744(5)
As–O4 = 1.677(5)	H3····O2 = 1.943(5)	Ba–O3 no. 3 = 2.795(5)
O1–H1 = 0.8203	O1····O2 = 2.666(7)	Ba–O4 no. 4 = 2.803(5)
O2–As–O1 = 102.7(2)	Ow····O4 = 2.705(7)	Ba–O3 no. 5 = 2.815(5)
O4–As–O1 = 106.3(3)	Ow····O2 = 2.704(7)	Ba–Ow no. 6 = 2.927(5)
O3–As–O1 = 108.6(2)	O4····Ow····O2 = 117.08	
O3–As–O4 = 109.2(3)	O1–H1····O2 = 98.48(0.38)	
O2–As–O4 = 114.2(2)	Ow–H2····O4 = 140.8(3)	
O3–As–O2 = 115.0(3)	Ow–H3····O2 = 128.7(3)	

Notes: No. 1 = $-x + 1/2, -y, z - 1/2$; no. 2 = $-x - 1/2, y + 1/2, z$; no. 3 = $-x, -y, -z$; no. 4 = $x - 1/2, -y + 1/2, -z$; no. 5 = $x - 1, y, z$; no. 6 = $x - 1, -y + 1/2, z - 1/2$. Hydrogen bridges are denoted by points (····).

chains are interconnected by the O1-H1···O2 hydrogen bridges to form ≈ 6 Å thick slices parallel to (001). Figure 2b shows one of these "H_2O–[$HAsO_4$]" slices projected onto (001). It is worth noting that the hydrogen-bonding is distributed in slices parallel to (001), but there are no hydrogen bridges linking O atoms that belong to different slices.

While these "H_2O–[$HAsO_4$]" slices are useful to describe the distribution of hydrogen bonds, they are not relevant from the point of view of the attractive electrostatic forces between $[HAsO_4]^{2-}$ and Sr^{2+}. A complementary picture of the structure can be obtained by considering the framework formed by [SrO_7] polyhedra and arsenate tetrahedra. The [SrO_7] polyhedra are linked to [$HAsO_4$] groups into slices that are also parallel to (001). These "[SrO_7]–[$HAsO_4$]" slices are connected in the [001] direction by hydrogen bonds from the water molecules. This is clear in Figure 3, where the interconnected "H_2O–[$HAsO_4$]" and "[SrO_7]–[$HAsO_4$]" slices are projected onto (100). Al-

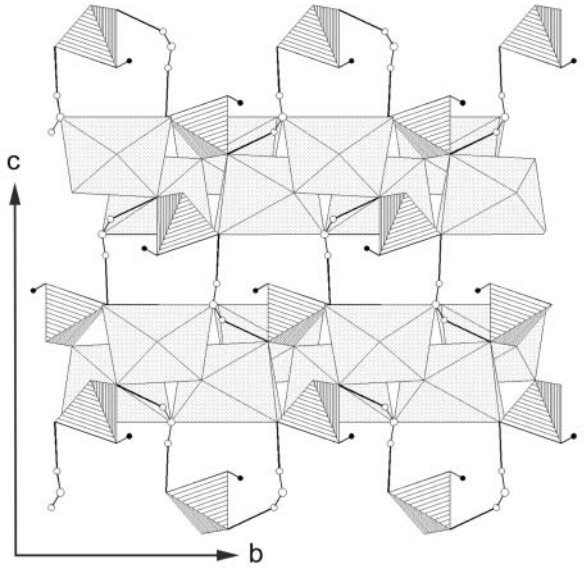

FIGURE 3. Projection of the $SrHAsO_4·H_2O$ structure onto (100). Both "H_2O–$[HAsO_4]$" and "$[SrO_7]$-$[HAsO_4]$" slices can be seen. Hydrogen bonds involving water hydrogen atoms (small open circles) are represented by thick solid lines. Hydrogen bonds involving anionic hydrogen atoms (black circles) are not represented in this plot.

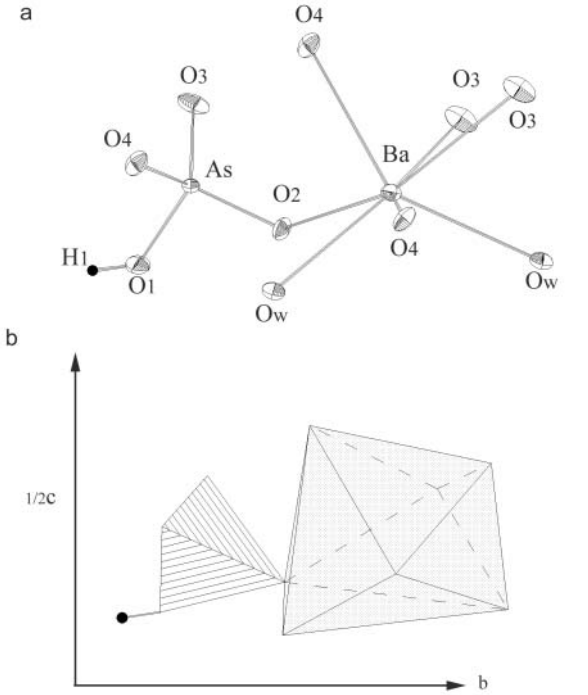

FIGURE 4. Projection onto (100) of a region of the $BaHAsO_4·H_2O$ structure. The O1 atom of the arsenate group is attached to H1, thereby forming the acidic aresenate $[HAsO_4]^{2-}$ group. The barium atom is surrounded by five arsenate O atoms and by two Ow atoms of water molecules. (**a**) ORTEP-style plot. (**b**) Arsenate tetrahedron and seven-apex polyhedron around barium. The anionic hydrogren atom (black circle) is also represented.

though some electrostatic interaction between Sr^{2+} cations and $[HAsO_4]^{2-}$ groups from adjacent slices is to be expected, the distance between the nearest As and Sr atoms from different slices is 4.52 Å, which is quite long compared with the typical (3.57–3.85 Å) distances between neighboring Sr and As atoms in the same slice (Table 4). Moreover, in the acid-arsenate tetrahedra, the hydroxyl O1-H1 apices are the nearest to the strontium atoms of the adjacent slice (see Fig. 3), with an O1-Sr distance of ≈3 Å. This means that the electrostatic interaction between adjacent $[SrO_7]$–$[HAsO_4]$ slices is mainly supported by the hydroxyl apices of the arsenate tetrahedron.

The structure of the Sr-rich ($Sr_{0.89}Ba_{0.11}HAsO_4·H_2O$) solid-solution crystal is essentially the same as that of the strontium end-member, with only minor differences in angles and distances. However, by considering in detail the configuration of the $[HAsO_4]^{2-}$ group, the crystal structure of the $BaHAsO_4·H_2O$ end-member appears to be different. While the tetrahedron in the $[HAsO_4]^{2-}$ group is similar in both end-members, the relative position of the anionic hydrogen atom is significantly different (Figs. 1 and 4). As in $SrHAsO_4·H_2O$, the As-O1 distance (1.753 Å) in the barium end-member is clearly longer than the other three As-O distances in the arsenate group, which results in an irregular tetrahedron with O-As-O angles ranging from 102.7 to 115.0° (Fig. 4 and Table 6). Similarly, the anionic hydrogen atom H1 is attached to the O atom farthest from the arsenic atom the tetrahedron. The location of this hydrogen atom with respect to the tetrahedron is, however, rather different in both structures. Finally, each barium atom is surrounded by a seven-apex polyhedron of O atoms that is considerably larger than the $[SrO_7]$ polyhedron in the $SrHAsO_4·H_2O$ structure, which is a consequence of the larger ionic radium of Ba^{2+} (1.38 Å) compared to Sr^{2+} (1.21 Å).

The location of the anionic hydrogen atoms has a significant influence on the hydrogen-bonding network in the structures of the two end-members. While the arrangement of hydrogen bonds involving water molecules is essentially the same, the structural role of the anionic hydrogen atom is different. In the $BaHAsO_4·H_2O$ structure, the water molecules connect with arsenate groups to form zigzag chains (Fig. 5a) that are similar to those shown in Figure 2a for $SrHAsO_4·H_2O$. However, in the barium end-member, these chains appear not to be interconnected by O1-H1···O2 bridges (Fig. 5b) to form slices parallel to (001). While the O1···O2 distance (2.67 Å) is similar to the donor-acceptor O1···O2 distance (2.64 Å) observed in the strontium end-member (compare Tables 4 and 6), due to the position of the anionic H1 atoms in the $BaHAsO_4·H_2O$ structure, the distance from H1 to the nearest O2 atom of the next arsenate tetrahedron is very long (H1···O2 = 2.418 Å) and the O1-H1····O2 angle (98.48°) is very far from 180°. These features suggest that hydrogen bonding involving H1 is not operating in the Ba end-member, which become more evident if one considers the bond-strength-bond-length relationship and the electrostatic-valence balance (Catti and Ferraris 1973) concerning the O atoms in this structure. To correlate bond strengths and bond lengths Brown and Shannon (1973) use the expression:

$$s = \left(\frac{R}{R_o}\right)^{-N} \quad (1)$$

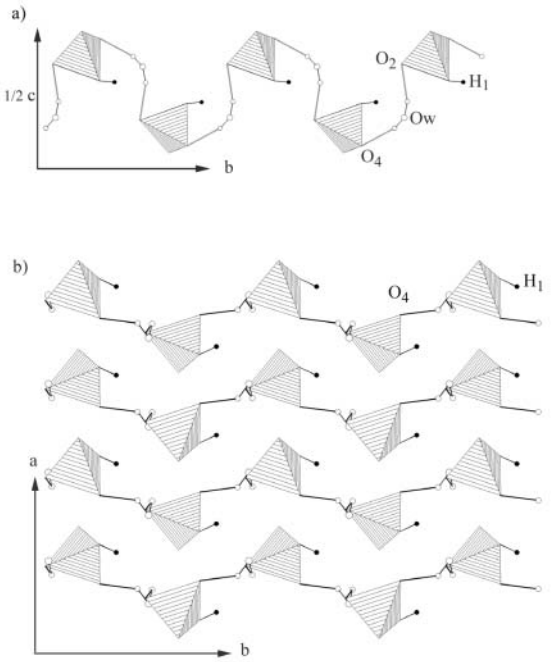

FIGURE 5. Hydrogen bonds in the $BaHAsO_4 \cdot H_2O$ structure. (**a**) Arsenate groups and water molecules link to form zigzag chains along [010]. (**b**) Projection of the zigzag chains on (001). There is no hydrogen bond involving anionic hydrogen atoms (balck circles). Hydrogen bonds involving water hydrogen atoms (small open circles) are represented by thick solid lines.

where s and R are, respectively, the bond strength and the bond length and R_o and N are fitted constants. The sum (p_i) of the bond strengths around the atom i is given by:

$$p_i = \sum_j s_{ij} \tag{2}$$

Here, the value of this sum has been obtained for the O atoms in both $BaHAsO_4 \cdot H_2O$ and $SrHAsO_4 \cdot H_2O$ by computing the bonding strengths with the neighboring As, Ba (or Sr), and H1 (in the case of O1), according to Equation 1. The values of R_o and N used in this calculation are from Brown and Shannon (1973) and the parameter R corresponds to the experimental As-O distances reported in Tables 4 and 6. The results show that the O1 atom of the strontium end-member is clearly overbonded (p = 2.434 valence units) while the other three O atoms show lower values of p, namely 1.57, 1.90, and 1.86 v.u. for O2, O3, and O4, respectively. In contrast, in the Ba end-member the value of p corresponding to O1 is very close to 2 (2.085 v.u.), the other three values being comparable to those of the Sr end-member (1.58, 1.95, and 1.80 v.u. for O2, O3, and O4, respectively). This result indicates that the O1 in the $BaHAsO_4 \cdot H_2O$ structure is not sufficiently overbonded to act as a donor O atom, which seems to confirm the lack of hydrogen bonding involving the acidic hydrogen atom H1 in this end-member.

Figure 6 shows a projection onto (100) of the $BaHAsO_4 \cdot H_2O$ structure. The [BaO_7] polyhedra are linked to acid-arsenate groups to form slices parallel to (001). As in the strontium end-member, these "[BaO_7]–[$HAsO_4$]" slices are connected in the

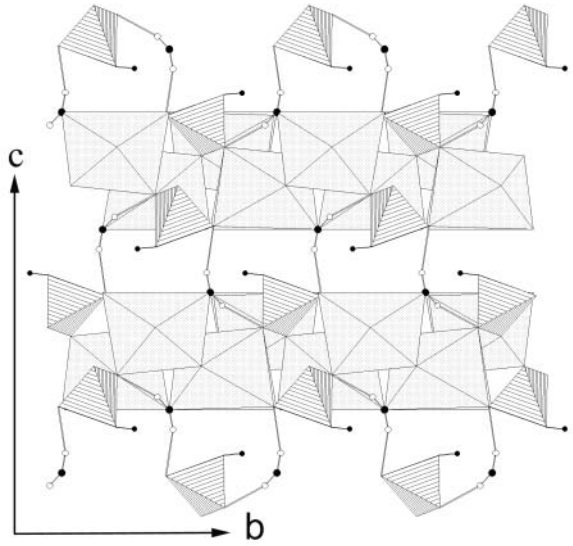

FIGURE 6. Projection of the $BaHAsO_4 \cdot H_2O$ structure onto (100). Both zigzag "H_2O-[$HAsO_4$]" chains and "[BaO_7]-[$HAsO_4$]" slices are shown. Hydrogen bonds involving water hydrogen atoms (small open circles) are represented by thick solid lines.

[001] direction by hydrogen bonds from the water molecules, such that the projection has a general aspect that is similar to that shown in Figure 3 for $SrHAsO_4 \cdot H_2O$. The distance (≈ 4.60 Å) between the nearest As and Ba atoms from adjacent slices is longer than the corresponding As-Sr distance (4.52 Å) in the Sr end-member. Similarly, the distance from the hydroxyl apices of the tetrahedra to the nearest barium atom of the adjacent slice is O1-Ba ≈ 3.1 Å, i.e., 0.1 Å longer than the corresponding O1-Sr distance in the structure of the strontium end-member. In contrast, the H1-Ba distance is ≈ 3.01 Å from the hydrogen atom of these hydroxyl apices to the nearest barium atom, which is considerably shorter than the corresponding H1-Sr ≈ 3.37 Å distance in the $SrHAsO_4 \cdot H_2O$ structure. This is a consequence of the relative position of H1 in the $BaHAsO_4 \cdot H_2O$ structure, which is displaced toward the free space between adjacent [BaO_7]–[$HAsO_4$] slices. All these features seem to suggest that the electrostatic interaction between adjacent [BaO_7]–[$HAsO_4$] slices is weaker than the interaction between adjacent [SrO_7]–[$HAsO_4$] slices in $SrHAsO_4 \cdot H_2O$.

Crystal morphologies and crystallization behavior

Table 7 compiles the composition of the precipitating crystals as a function of the initial concentration of the parent aqueous solutions. The solid-phase compositions are expressed in terms of the mole fraction (X_{Ba}) of the $BaHAsO_4 \cdot H_2O$ component in the solid solution. These values were obtained by EDX microanalysis and are average values corresponding to 5 different crystals of the same precipitate, the standard deviation being always less than ±0.05. The fluid compositions of the parent solutions are also expressed in terms of the relative molar fraction ($X_{Ba,aq}$) of dissolved barium, i.e.,

$$X_{Ba,aq} = \frac{[Ba^{2+}]}{[Ba^{2+}] + [Sr^{2+}]} \tag{1}$$

TABLE 7. Initial concentration of the parent solution, nucleation data, and cell parameters for the (Sr,Ba)$HAsO_4 \cdot H_2O$ solid solution

Parent solutions (M)		$X_{Ba,aq}$	X_{Ba}	a (Å)	b (Å)	c (Å)
$SrCl_2$	$BaCl_2$					
0.1	0	0	0	7.436	8.481	14.348
0.2	0.01	0.048	0.11	7.443	8.478	14.385
0.1	0.01	0.091	0.42	7.473	8.481	14.351
0.1	0.05	0.33	0.63	7.606	8.599	14.511
0.1	0.066	0.40	0.77	7.757	8.728	14.626
0.1	0.1	0.50	0.76	7.673	8.702	14.610
0.09	0.1	0.53	0.79	7.726	8.730	14.630
0.066	0.1	0.60	0.89	7.750	8.752	14.645
0.01	0.1	0.91	0.99	7.751	8.769	14.659
0	0.1	1	1	7.752	8.759	14.668

where the terms in brackets represent the total concentrations of the substituting ions in the parent solution. These $X_{Ba,aq}$-X_{Ba} pairs can be used to construct a $X_{Ba,aq}$-X_{Ba} plot as shown in Figure 7a, which illustrates the distribution of the substituting ions during the whole diffusion-crystallization process. In this figure, the data points have been fitted (dashed line) to a function of the type:

$$X_{Ba} = \frac{P_1 X_{Ba,aq}}{(P_1 - P_2)X_{Ba,aq} + P_2} \quad (2)$$

where P_1 and P_2 are variable fitting parameters (Prieto et al. 1997). In this case the best fit was obtained for $P_1 = 2.89 \times 10^{-5}$ and $P_2 = 6.95 \times 10^{-6}$. As we will discuss later, this plot has only a phenomenological meaning because it includes contributions of the thermodynamics of the solid-solution/aqueous-solution (SS-AS) system but also transport and kinetics effects. In any case, the fitting function shown in Equation 2 allows for the estimation of a rough, "operative" distribution coefficient for the present experiments, given by:

$$D_{Ba} = \frac{X_{Ba}}{1 - X_{Ba}} \Big/ \frac{X_{Ba,aq}}{1 - X_{Ba,aq}} = \frac{P_1}{P_2} = 4.16 \quad (3)$$

As can be observed, during the whole process there is a preferential incorporation of barium into the solid phase: solid solutions of intermediate compositions ($X_{Ba} = 0.50$) crystallize from parent solutions that are moderately Sr-rich ($X_{Ba,aq} \approx 0.19$).

Both Table 7 and Figure 7b display evolution of the unit-cell size with the crystal composition. The cell parameters corresponding to the intermediate solid solutions were obtained from the powder-diffraction diagrams. As can be observed, the unit-cell size increases with the barium content. This increase is clearly non-linear, the enlargement being moderate in the strontium-rich region and then increasing significantly for compositions in the range $0.4 < X_{Ba} < 0.7$. Finally it increases in a moderate way on the barium-rich side.

Figures 8a and 8b show, respectively, the typical morphologies of $SrHAsO_4 \cdot H_2O$ and $BaHAsO_4 \cdot H_2O$ single crystals. As can be observed, in both cases the crystal morphology is dominated by {001} followed by {102}, {111}, {112}, {021}, and {100} as secondary faces. All these forms correspond to structural planes that are the most important according to the Donnay-Harker (1937) rules. Although the Donnay-Harker method is only an approximation, it is useful to estimate in a qualitative way the morphological importance of crystal forms. Thus, for the strontium term, the D-H method ranks {002} first, with a reticular area of 14.872 Å^2. The forms {111}, {102}, {112}, {020}, {021}, and {100} follow, but the reticular areas of the corresponding structural planes are significantly larger (20.480, 20.665, 24.195, 25.161, 26.238, and 28.696 Å^2, respectively).

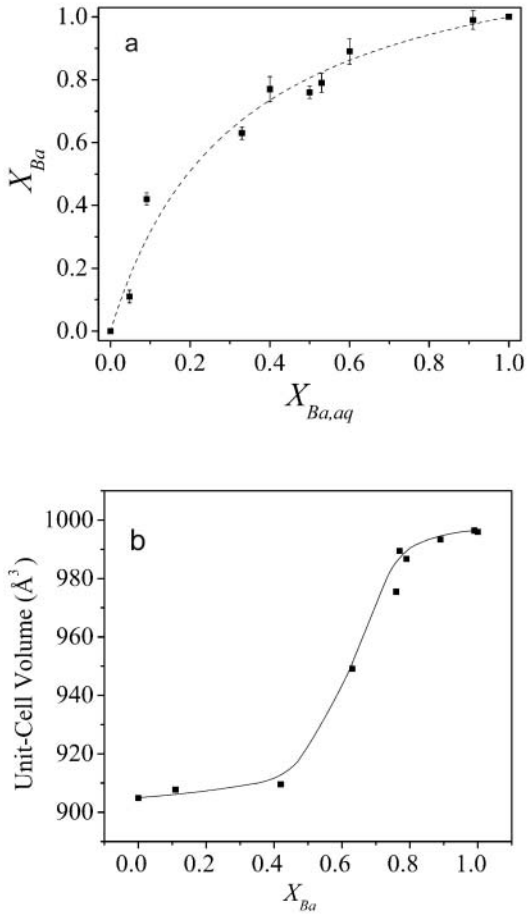

FIGURE 7. (**a**) Experimental X_{Ba}-$X_{Ba,aq}$ pairs. A curve fitting the experimental points has been computed according to Equation 2. (**b**) Dependence of the unit-cell volume on composition of the solid phases.

While the forms observed in both end-members are essentially the same, the relative development of these forms is significantly different. The preponderance of {001} is especially marked in the $BaHAsO_4 \cdot H_2O$ crystals, which exhibit tabular or lamellar shapes with wide (001) faces. In this end-member, the easy cleavage on {001} leads to a flaky appearance, due to the crystal splitting into (001) flakes. This is clear in Figure 9, which shows the typical habits of three different compositional terms of this solid-solution. As can be observed, the flaky appearance increases with the barium content.

DISCUSSION

The previous data indicate that $SrHAsO_4 \cdot H_2O$ and $BaHAsO_4 \cdot H_2O$ form a complete solid-solution where Sr^{2+} ions substitute for Ba^{2+}. Both end-members crystallize in the same orthorhombic *Pbca* space group, with lattice parameters that vary significantly with composition. The cell volume increases from 904.8(5) to 996.2(2) Å, which is not surprising if one considers the difference

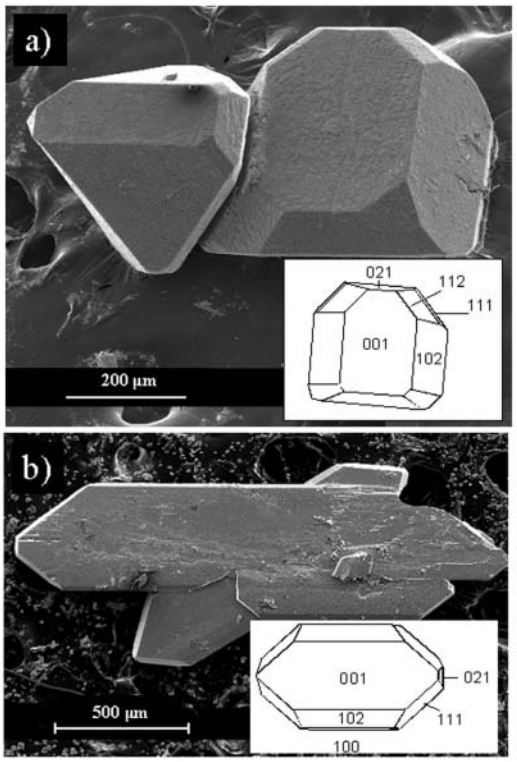

FIGURE 8. Electron microphotograph of (**a**) $SrHAsO_4{\cdot}H_2O$ and (**b**) $BaHAsO_4{\cdot}H_2O$ crystals. The corresponding crystal forms are shown in the inserts.

of ionic radii for Sr^{2+} (1.21 Å) and Ba^{2+} (1.38 Å). In spite of these similarities, the end-members are not exactly isostructural. While the heavy atoms are arranged in comparable general positions, there are significant differences in the position of the anionic hydrogen atoms H1 and consequently in the hydrogen-bonding network. In the $SrHAsO_4{\cdot}H_2O$ structure, both the water hydrogen atoms and the anionic hydrogen atoms are involved in hydrogen bridges, with a total of three hydrogen bonds per unit formula. In contrast, there are no hydrogen bonds involving H1 in the $BaHAsO_4{\cdot}H_2O$ structure, resulting in this end-member having only two hydrogen bonds per unit formula. On the other hand, both end-members have a layered structure with slices parallel to (001) that contain Sr^{2+} or Ba^{2+} ions and $[HAsO_4]^{2-}$ groups (see Figs. 3 and 6). Although some electrostatic interaction between adjacent (001) slices is to be expected, these layers are mainly linked by hydrogen bonds from the water molecules between them. In any case, the inter-atomic distances suggest that the electrostatic interaction between adjacent slices is weaker in $BaHAsO_4{\cdot}H_2O$ than in $SrHAsO_4{\cdot}H_2O$. These features account for both the perfect cleavage on {001} and the higher morphological importance of this form in the Ba end-member. Finally, the fact that the unit-cell parameters vary in a non-linear way with the solid composition is consistent with the structural differences between both end-members and point toward a non-ideal character of the solid solution.

From the point of view of the crystallization behavior, all data seem to indicate that there is a preferential partitioning

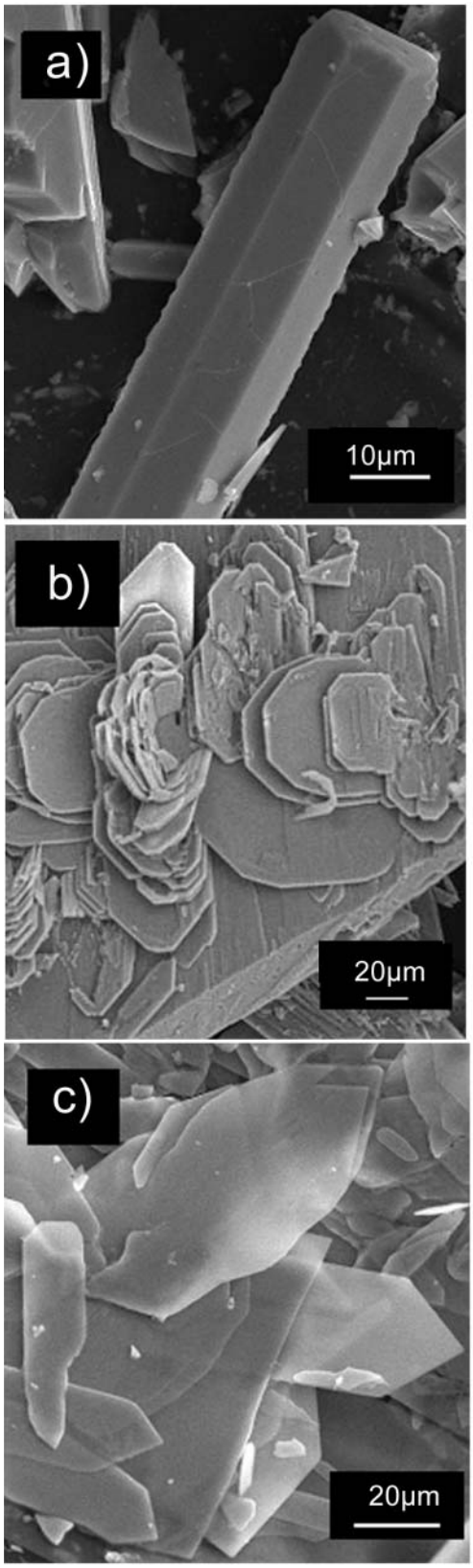

FIGURE 9. Growth habits of (**a**) $SrHAsO_4{\cdot}H_2O$, (**b**) $Sr_{0.23}Ba_{0.77}HAsO_4{\cdot}H_2O$, and (**c**) $BaHAsO_4{\cdot}H_2O$.

of barium into the solid phase. Although the plot in Figure 7 includes effects derived from the different transport behavior of Ba^{2+} and Sr^{2+} throughout the gel column, this influence is expected to be small, given the small difference (≈3%) between the diffusivities of $BaCl_2$ and $SrCl_2$. Therefore, the $X_{Ba,aq}$ values compiled in Table 7 can be considered as a rough estimate of the fluid composition in the crystallization zone, by assuming that the barium/strontium proportion in the aqueous solution does not change drastically during the diffusion process. On the other hand, there is evidence from experimental data that hydrogels reduce the nucleation probability such that nucleation occurs when a significant supersaturation threshold is attained (Henisch 1988; Lefaucheux and Robert 1994; Prieto et al. 1994). Obviously, the composition of the crystals nucleating from the supersaturated solutions depends on kinetic factors, and the "effective" distribution coefficient differs from the equilibrium values. Numerous studies (Lorens 1981; Prieto et al. 1997; Fernández-González et al. 1999; Putnis et al. 2003) demonstrate that preferential partitioning is in some way decreased at high supersaturation, such that the equilibrium preferential partitioning of barium could be stronger than that shown in Figure 7. The determination of the equilibrium behavior in SS-AS systems requires knowledge of both the end-member solubility products and the degree of non-ideality of the solid-solution (Glynn and Reardon 1990). Unfortunately, the lack of thermodynamic data for arsenates is even greater than the lack of crystal-chemical data. In this particular case the solubility of the barium end-member has been determined by Itoh and Tozawa (1989), who find a *pK* value of 5.31. However, the solubility of the strontium end-member as well as the thermodynamic properties of the solid solution are unknown such that the present results can only be interpreted in a qualitative way. The fact that there is a significant preferential partitioning of barium toward the solid phase seems to indicate a lesser solubility (≈ one order of magnitude) for the strontium end-member. Moreover, both the deviations from the linearity of the cell parameters and the differences between the structures of the end-members seem to point toward a non-ideal miscibility. A thermodynamic study of the system is, however, beyond the scope of the present work, which is mainly focused on the crystal-chemical aspects. Future papers will deal with this matter.

ACKNOWLEDGMENTS

This work was partially supported by the Ministry of Science and Technology of Spain (grants BTE2000-0300 BQU2000-0219) and FICYT (Foundation for Applied Scientific Investigation and Technology of Asturias, Spain, grant GE-EXP01-02). We thank D. Heasman for his insightful comments. Electron microscopy and X-ray diffraction were carried out by Central Scientific Services of the University of Oviedo. Drafts of this manuscript were much improved by the careful reviews of A. Gualteri, G. Ferraris, and R. Downs.

REFERENCES CITED

Beurskens, P.T., Admiraal, G., Beurskens, G., Bosman, W.P., Garcia Granda, S., Gould R.O., Smits, J.M.M., and Smykalla, C. (1992) The DIRDIF program system. Technical Report of the Crystallography Laboratory, University of Nijmegen. The Netherlands.

Binas, H. and Boll-Dornberger, K. (1962) The structure of $CaHAsO_4·H_2O$ (haidingerite) and SrHAsO4·H2O. Chemie der Erde, 21, 450–452.

Brown, I.D. and Shannon, R.D. (1973) Empirical bond-strength-bond length curves for oxides. Acta Crystallographica B, 29, 266–282.

Catti, M. and Ferraris, G. (1973) Hydrogen bonding in the crystalline state. Crystal structure of $CaHAsO_4·3H_2O$. Acta Crystallographica B, 29, 90–96.

Donnay, J.D.H. and Harker, D. (1937) A new law of crystal morphology extending the law of Bravais. American Mineralogist, 22, 446–467.

Fernández González, A., Martín-Díaz, R., and Prieto, M. (1999) Crystallisation of $Ba(SO_4,CrO_4)$ solid solutions from aqueous solutions. Journal of Crystal Growth, 200, 227–235.

Ferraris, G. and Chiari, G. (1970) Crystal structure of disodium hydrogen orthoarsenate heptahydrate, $Na_2HAsO_4·7H_2O$. Acta Crystallographica B, 26, 1574–1583.

Ferraris, G., Jones, D.W., and Yerkess, J. (1971a) Neutron diffraction study of the crystal structure of sodium arsenate heptahydrate $Na_2HAsO_4·7H_2O$. Acta Crystallographica B, 27, 354–359.

——— (1971b) Determination of hydrogen atom positions in the crystal structure of pharmacolite, $CaHAsO_4·2H_2O$, by neutron diffraction. Acta Crystallographica B, 27, 349–354.

——— (1972) Neutron and X-ray refinement of the crystal structure of $CaHAsO_4·H_2O$ (haidingerite). Acta Crystallographica B, 28, 209–214.

Glynn, P.D. and Reardon, E.J. (1990) Solid-solution aqueous-solution equilibria: Thermodynamic theory and representation. American Journal of Science, 290, 164–201.

Grant, D.F. and Gabe, E.J. (1978) The analysis of single-crystal Bragg reflections from profile measurements. Journal of Applied Crystallography, 11, 114–120.

Henisch, H.K. (1988) Crystals in gels and Liesegang rings. Cambridge University Press, U.K.

Itoh, C.T. and Tozawa, K. (1989) Equilibria of the barium(II)-arsenic(III, V)-water system at 25ºC. Tohoku Daigaku Senko Seiren Kenkyusho Iho, 45, 105–116.

Lefaucheux, F. and Robert, M.C. (1994) Crystal growth in Gels. In D.T.J. Hurle, Ed., Handbook of Crystal Growth, vol. 2, p. 1271–1303. North-Holland, Amsterdam.

Lehman, M.S. and Larsen, F.K. (1974) A method for location of the peaks in step-scan measured Bragg reflexions. Acta Crystallographica A, 30, 580–584.

Lorens, R.B. (1981) Strontium, cadmium, manganese, and cobalt distribution coefficients in calcite as function of calcite precipitation rate. Geochimica et Comochimica Acta, 45, 553–561.

Martin, C., Durif, A., and Averbuch-Pouchot, M.T. (1970) Sur le groupe spatial de l'haidingerite. Données cristallographiques sur $BaHAsO_4H_2O$. Bulletin Societe Francaise Mineralogie Cristallographie, 93, 397–398.

Nardelli, M. (1983) PARST: a system of FORTRAN routines for calculating molecular structure parameters from results of crystal structure analyses. Computers and Chemistry, 7, 95–98.

Nriagu, J., Ed. (1994) Arsenic in the environment, 430 p. Wiley, New York.

Parkin, S., Moezzi, B., and Hope, H. (1995) XABS2: an empirical absorption correction program. Journal of Applied Crystallography, 28, 53–56.

Planer-Friedich, B., Armienta, M.A., and Merkel, B.J. (2001) Origin of arsenic in the groundwater of the Rioverde basin, Mexico. Environmental Geology, 40, 1290–1298.

Prieto, M., Putnis, A., Fernández-Diaz, L., and López Andrés, S. (1994) Metastability in diffusing-reacting systems. Journal of Crystal Growth, 142, 225–235.

Prieto, M., Fernández González, A., Putnis, A., and Fernández-Diaz, L. (1997) Nucleation, growth and zoning phenomena in crystallizing $(Ba,Sr)CO_3$, $Ba(SO_4,CrO_4)$, $(Ba,Sr)SO_4$, and $(Cd,Ca)CO_3$ solid solutions from aqueous solutions. Geochimica et Cosmochimica Acta, 61, 3383–3397.

Putnis, A., Pina, C.M., Astilleros, J.M., Fernández Díaz, L., and Prieto, M. (2003) Nucleation of solid solutions crystallizing from aqueous solutions. Philosophical Transactions A of the Royal Society London, 361, 615–632.

Sheldrick, G.M. (1997) SHELXL97: Program for the Refinement of Crystal Structures. University of Göttingen: Göttingen, Germany, 1997.

Smedley, P.L. and Kinniburgh, D.G. (2002) A review of the source, behaviour and distribution of arsenic in natural waters. Applied Geochemistry 17, 517–568.

MANUSCRIPT RECEIVED JUNE 4, 2003
MANUSCRIPT ACCEPTED OCTOBER 23, 2003
MANUSCRIPT HANDLED BY ALESSANDRO GUALTIERI